Cite this: DOI: 10.1039/xxxxxxxxxx

Received Date
Accepted Date

DOI: 10.1039/xxxxxxxxxx

www.rsc.org/journalname

Capillary induced twisting of Janus cylinders

Alexandros T. Oratis, Timothy Farmer and James C. Bird*

At the appropriate length scales, capillary forces exerted by a liquid in contact with a compliant solid can cause the solid's deformation. Capillary forces are also able to align particles with discrete wettabilities – or Janus particles – at liquid interfaces. Their amphiphilic properties enable Janus particles to orient themselves at liquid interfaces such that both of their surfaces are facing their preferred fluid. However, it is unclear how to spontaneously obtain varying degrees of rotational alignment. Here we extend ideas of elasto-capillarity to modulate rotational alignment by connecting amphiphilic Janus cylinders in an antisymmetric configuration. As the Janus cylinders rotate they cause a twisting deformation of rod. We develop both a mathematical model and a physical macroscale setup to relate the angle of twist to the elastic and interfacial properties, which can be used to tune the extent of alignment of Janus particles at air-water interfaces. We additionally extend our analysis to calculate the twist profile on a compliant element with a distributed capillary torque.

Introduction

When a liquid comes into contact with a compliant solid, surface tension can significantly bend and deform the solid. For example, surface tension has been shown to cause the folding of elastic structures[1,2], wrinkling patterns on thin sheets[3,4] and snap-through instabilities[5]. In this field of elasto-capillarity, the amount of deformation is determined by a balance of surface tension and the resisting elastic forces of the solid[6]. Meanwhile, surface tension is also responsible for the adhesion of solid particles at immiscible fluid interfaces[7,8]. This adhesion can be enhanced if the particles themselves have two distinct surface wettabilities, such as a hydrophobic face and a hydrophilic face[9,10]. Particles with two faces, referred to as Janus particles, can spontaneously orient themselves at a fluid interface such that the hydrophobic and hydrophilic surfaces are each surrounded by their preferred fluid. This fully aligned orientation can be used to increase the stability of emulsions[11,12], as well as align optical or chemical features associated with the Janus faces[13,14]. However, in cases in which it is advantageous to restrict the alignment of Janus particles at liquid interfaces, it is not immediately clear how to passively modulate the fraction of each face exposed to its preferred fluid. To accomplish this goal, we pursue an elasto-capillary approach in which elastic compliance is varied to temper the rotational alignment of Janus particles.

An amphiphilic Janus cylinder placed at an air-water interface with the hydrophobic side facing the water is unstable and a small rotational perturbation will reduce the total interfacial energy (Fig. 1a)[15]. This change in energy with rotation manifests as a torque exerted on the cylinder via capillary forces and—provided that the surfaces are sufficiently smooth—can rotate the particle[16].

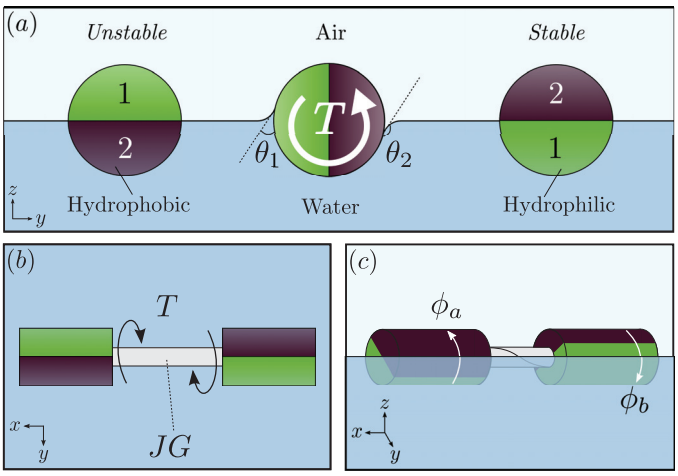

Fig. 1 Alignment of Janus particles with discrete wettabilities at an air-water interface. ***a*** Schematic portraying the stability of a particle that is partially coated with a hydrophilic material 1 and partially coated with a hydrophobic material 2, when placed at a liquid interface. When the particle is not in an equilibrium position, the hydrophilic surface makes a contact angle θ_1 with the water while the hydrophobic surface makes a contact angle θ_2. This difference in contact angle difference induces a torque T that tends to rotate the particle. ***b*** Top view of two Janus cylinders connected by a flexible rod with torsional stiffness JG placed at a liquid interface. ***c*** Schematic of the final configuration of the tethered cylinders in which both cylinders have rotated by angles ϕ_a and ϕ_b respectively.

Department of Mechanical Engineering, Boston University, Boston, MA 02215, USA; E-mail: jbird@bu.edu

Although Janus particles can be actively perturbed from their equilibrium alignment in the presence of external shear flows[17,18], we are unaware of passive alignment techniques. Here we demonstrate a way in which the rotational alignment of Janus particles could be passively tuned through elasto-capillary twist. Specifically, we show that an imbalance of capillary forces from the discrete surface wettabilities can lead to a torque onto a connecting rod (Fig. 1b). Depending on the compliance of the rod, the capillary torque will rotate the Janus cylinders relative to one another by varying degrees (Fig. 1c). Thus we find that the fraction of the solid surface exposed to its preferred phase can be tuned by modulating the material and geometric properties that determine the elasto-capillary twist.

Methods

To explore how material and geometric properties can lead to a capillary-induced twist, we carry out macroscale experiments based on the initial antisymmetric wetting configuration illustrated in Figure 1. Centimeter-scaled Janus cylinders are made by partially coating a glass vial with candle soot. To accomplish the Janus patterning, half of the surface area is masked with tape. After the entire vial is covered with candle soot, the tape is removed, leaving half of the glass surface uncoated. The advantage of soot over other coatings is that it is both superhydrophobic and black; these characteristics help visually identify the boundary of the coating and provide a large contrast in wettability. The contact angles that the uncoated glass and candle soot make with water, were experimentally measured by placing an uncoated vial and a fully soot coated vial in a water bath. The corresponding macroscopic contact angles were measured by inspection to be $\theta_1 \approx 70^\circ$ and $\theta_2 \approx 150^\circ$ respectively (Fig. 2a). These values were consistent with independent measurements obtained for a small drop of water on a coated and uncoated glass slide. Further contact angle measurements confirmed that the tape removal process did not affect the contact angle of the glass. We attach the two Janus cylinders with a flexible rod that we fabricate from cross-linked polydimethylsiloxane (PDMS). Using glass vials as our Janus cylinders is advantageous as they contain caps through which we can drill a centered hole. We pass each end of the PDMS rod through a tight fitting hole in the corresponding vial cap and secure the rod within the vial with epoxy. In the experiments, the radius r and length ℓ of the connecting rods are varied; whereas, the size of the Janus cylinders remain fixed (radius $R = 6$ mm and length $L = 2.5$ cm). In addition, the shear modulus G of the rod is varied by tuning the amount of curing agent added to the PDMS during the fabrication process (20:1, 10:1, 5:1 polymer/curing agent mix). To measure the shear modulus, we conducted cantilever tests on rectangular PDMS strips that were fabricated following the same procedures as the PDMS rods. In these tests, the tip deflection is measured for varying strip lengths and from these deflections a shear modulus is calculated following beam theory (Fig. 2b).

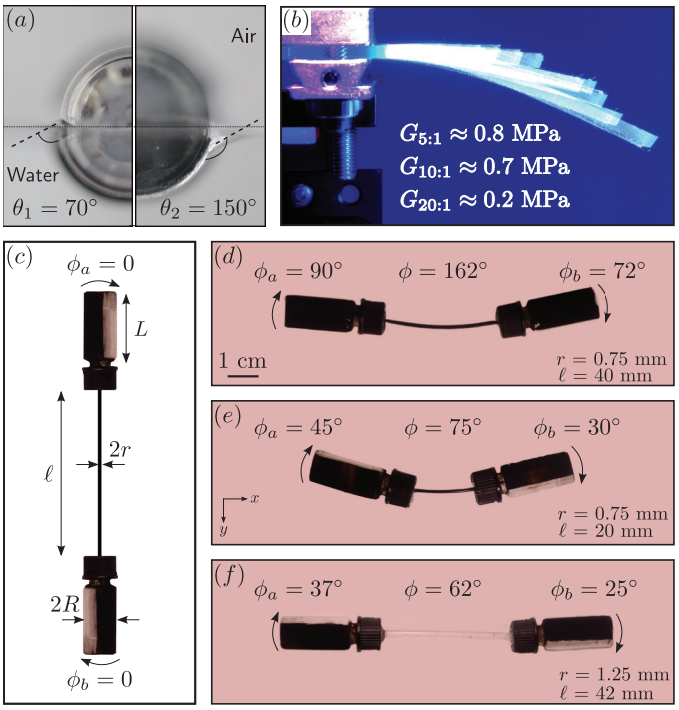

Fig. 2 Effect of the geometrical and material properties of the PDMS rod on the rotation of the Janus cylinders. ***a*** Two half-photographs of an uncoated glass vial (left) and a soot-coated vial (right) at an air-water interface revealing the contact angles $\theta_1 \approx 70^\circ$ and $\theta_2 \approx 150^\circ$ respectively. ***b*** Superimposed images of PDMS cantilever strips with varying tip deflections used to compute the shear moduli G. ***c*** Schematic of macromodel geometry, portraying the partially coated vials with lengths L and radii R connected by the rod with length ℓ and radius r. ***d-f*** Images of the equilibrium configurations for rods with varying radii and lengths and fixed shear modulus $G = 0.2$ MPa.

The macroscale experiments consist of gently placing the tethered Janus cylinders on an air-water interface and observing the equilibrium rotational alignment of the cylinders. A top view of the untwisted experimental configuration is depicted in Figure 2c. As the tethered cylinders are placed in this configuration on an air-water interface, they are free to rotate as they float, half submerged on the interface. The amount of rotation of each cylinder can be measured by noting the fraction of the black soot surface observed from the top view of the interface (Fig. 2d-f). Specifically from trigonometry, the rotation angle of Janus cylinder i is related to the projected soot breadth B_i as $\phi_i = 90^\circ - \cos^{-1}[(B_i/R) - 1]$, where $B_i/2R$ is the observed soot fraction. If the cylinders rotate completely, that is if they rotate so that the uncoated glass is in full contact with the water and the soot with air, then only the black soot would be visible from the top view ($B_i = 2R$) and thus the angles of rotation of each cylinder, ϕ_a and ϕ_b, would be 90°. Whereas, if the cylinders do not rotate completely, then a portion of both the uncoated glass and the soot faces are visible from the top view and $B_i < 2R$. Because the rotation of these cylinders directly twist the ends of the compliant elastomer rod, it is perhaps more instructive to focus on a single parameter, the rod twist angle, $\phi = \phi_a + \phi_b$. For a connecting rod with radius $r = 0.75\,\mathrm{mm}$, length $\ell = 40\,\mathrm{mm}$ and shear modulus $G = 0.2\,\mathrm{MPa}$ (Fig. 2d), the rod offers minimal resistance to the rotation of the Janus cylinders, and the resulting twist angle is near the maximum value of $\phi = 180^\circ$. Decreasing the rod's length by a half reduces the twist, as does increasing the rod's radius (Fig. 2e,f).

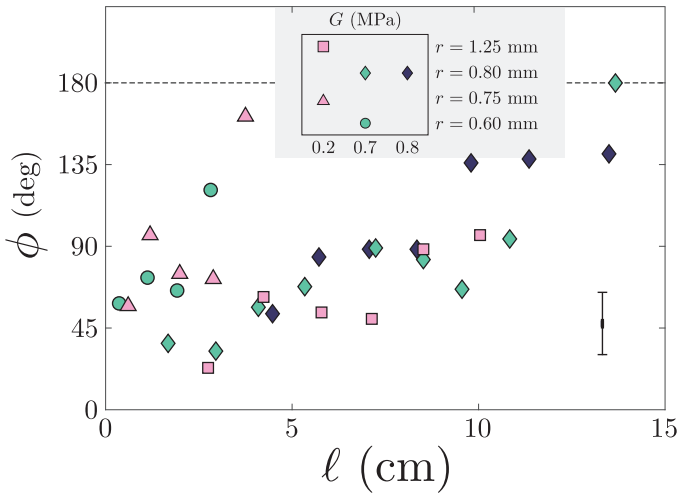

Fig. 3 Experimental results of the equilibrium twist angle ϕ plotted against the length of the rod ℓ for varying geometrical and material properties. The dotted line indicates the maximum angle of twist that can be achieved $\phi = 180°$. Inset shows the different radii r and shear moduli G combinations corresponding to the plotted data points. Representative error bars for the data points are shown in the bottom right corner.

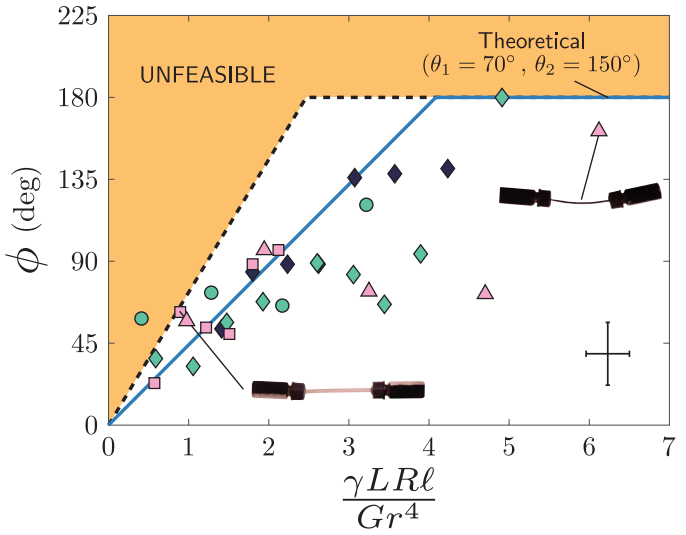

Fig. 4 Twist angle data rescaled against the dimensionless group $\gamma LR\ell/Gr^4$. The solid line denotes the model solution based on the contact angles of the surfaces used in experiments $\theta_1 = 70°$ and $\theta_2 = 150°$. Dotted line denotes the extent of the region that could theoretically be achieved for Janus cylinders and is based on perfectly wetting and nonwetting surfaces with contact angles $0°$ and $180°$.

Results and discussion

Experimental results

Depending on the properties of the PDMS rod once at the air-water interface, there is a wide range in the angle of twist and, by extension, rotation of each Janus cylinder. Figure 3 depicts the results of individual experiments in which the angle of twist ϕ is plotted as a function of the rod length ℓ for varying rod radii r and shear moduli G. The maximum angle of spontaneous twist is restricted to $180°$ (dotted line in Fig. 3); twists larger than $180°$ would increase both the surface and torsional energy due to the antisymmetric configuration on the surface. For rods with the same radii and shear moduli, increasing their lengths results in larger twists. By contrast, making the rods thicker or stiffer tends to decrease the twist. These trends would be expected if torsional stiffness is resisting the twist. Less clear is whether the amount of twist generated is consistent with the capillary torques available.

Theoretical model

To model the rod's twist, we consider the surface energy of the Janus cylinders E_s and the torsional energy of the rod E_t to be the dominant contributors to the angle of twist. For an incompressible neo-Hookean rod, the torsional energy is $E_t = GJ\phi^2/2\ell$, where $J = \pi r^4/2$ is the polar moment of inertia[19]. The capillary torque on the Janus cylinders can be calculated by the change in surface energy as it rotates. The surface energy is related to the surface area $E_s = \gamma_i A_i$, where γ_i is surface tension associated with the interface[20]. Thus, the change in the surface energy of the cylinder associated with the change in area from rotation can be expressed as $dE_s = \sum_i[(\gamma_{2V} - \gamma_{2L}) - (\gamma_{1V} - \gamma_{1L})]dA_i$, where γ_{2V} and γ_{2L} are the soot-vapor and soot-liquid surface tensions respectively, γ_{1V} and γ_{1L} are the glass-vapor and glass-liquid surface tensions respectively, and $dA_i = RLd\phi_i$ is the rotated surface area of each Janus cylinder. With the Young-Laplace law, the surface energy can be simplified to $dE_s = \gamma RL(\cos\theta_2 - \cos\theta_1)d\phi$, with γ denoting the surface tension of the air-water interface. Minimizing the total energy, $E = \int dE_s + E_t$ with respect to the twist angle ϕ, the equilibrium angle of twist is found to be:

$$\phi = \frac{\gamma RL\ell}{GJ}(\cos\theta_1 - \cos\theta_2) = \frac{2}{\pi}(\cos\theta_1 - \cos\theta_2)\frac{\gamma RL\ell}{Gr^4} \qquad (1)$$

Note that this relation could also be obtained with a torque balance between the cylinders subjected to equal and opposite capillary torques $T = \gamma RL(\cos\theta_1 - \cos\theta_2)$, connected by a torsional spring with stiffness GJ/ℓ.

Equation (1) reveals the importance of the dimensionless group $\gamma RL\ell/Gr^4$, which is linearly proportional to the angle of twist. The slope of this linear relationship is controlled by the surface angles of each Janus cylinder, through the term $\cos\theta_1 - \cos\theta_2$. In the event that the cylinders were of uniform wettability, that is $\theta_1 = \theta_2$, then the slope would be zero and, as expected, no twist would result. Alternatively, if the cylinders were perfectly wetting and nonwetting, that is $\theta_1 = 0°$ and $\theta_2 = 180°$, then the slope would reach a maximum of $4/\pi$. Therefore in addition to twist angles being limited to $180°$, the angles are further restricted if $\gamma RL\ell/Gr^4$ is less than $\pi^2/4$. Based on the wettability of our Janus cylinders, the theoretical slope is between these two extremes, as shown by the solid line in Figure 4.

Replotting the data points shown in Figure 3 onto these dimensionless axes, we find that they are consistent with our model and follow the trend of the theoretical solid line corresponding to Equation (1). Clearly there are deviations between the theory and experiments, which are not particularly surprising given the reductionist approach of our model. Yet the trend and order of magnitude of the results supports the notion that it is possible to twist a compliant rod with capillary torques or, alternatively, to restrain

the rotation of Janus cylinders with a compliant tether.

Model extension and limitation

Returning to the experimental images (Fig. 2d-f), it is clear that some of rods are curved when the angle of twist is measured, and it is natural to inquire whether this curvature has an effect on these measurements. To address this question, we incorporate previous analysis on the twisting of a curved circular bar[21] into our model. Specifically, both the torsional and bending energies are considered for a rod with constant curvature κ and torque confined to a plane. This analysis yields an additional term, $\{1 + [\nu/(2 + 2\nu)][(\sin(2\kappa\ell)/(2\kappa\ell) - 1]\}$, that is multiplied to the right-hand side of Equation 1. Here ν is the Poisson's ratio of the beam and is equal to 0.5 for PDMS[22]. We measure the curvature for all of our rods when ϕ is recorded and find that the largest value of κL is 0.22, which corresponds to a negligible correction of approximately 0.5%. Therefore, it appears that including bending in our model does not reduce the spread in the data. The source of the bending is not particularly clear. Sufficient twisting of slender rods has been shown to cause bending deformations in the form of helical torsional buckling[23,24], yet adapting these models to our system is non-trivial and beyond the scope of this study. Based on observations, we suspect that majority of bending arises from imperfections and perturbations in the system rather than twisting. Imperfections may also account for significant scatter in the measured angles. For example, contact angle hysteresis or errors in the alignment of the antisymmetric patterns during fabrication could modify the measured equilibrium twist angle.

Although we have presented a unique twist angle as a function of $\gamma RL\ell/Gr^4$, there is the potential for multiple equilibrium configurations if the rod were to contact the interface pretwisted by one or more full revolutions. If the capillary torque was not sufficient to maintain this twist, the energy balance suggests that the rod would unwind and reach the equilibrium twist angle calculated in Equation 1. However, if the capillary torque were able to maintain the twist, then the cylinders could rotate to a local energy minimum. A rod pre-twisted by a multiple of 360° would be able to withhold twists larger 180° as long as $\gamma RL\ell/Gr^4 > n\pi^2/(\cos\theta_1 - \cos\theta_2)$, with n denoting the number of full revolutions, and $\kappa\ell \ll 1$. Thus only if $\gamma RL\ell/Gr^4 > 8.2$ would we expect a full twist to be maintained for the contact angles in the experiments.

A limitation of our model is that it assumes rotation about the cylinder central-axis, which may not be the case if there are significant vertical displacements. To illustrate this limitation, we consider the case in which the Janus cylinders' surface is non-symmetrically hydrophobic and hydrophilic, which would correspond to a difference between the hydrophobic and hydrophilic surface areas. Quantifying the degree of non-symmetry by the fraction of the hydrophobic surface area over the total surface area of the cylinder as f, bounds f to a value between 0 (completely hydrophilic) and 1 (completely hydrophobic), with $f = 0.5$ corresponding to the symmetric Janus cylinders used in our experiments. Assuming rotations only about the central axis, the equilibrium angle of twist could still be described by Equation 1, but the maximum angle of twist would be confined to $\phi = 180^\circ(1 - |2f - 1|)$. However, if the tethering rod were sufficiently compliant, then the cylinders would be able to rotate further since the most energetically favorable state occurs when both hydrophobic and hydrophilic surfaces are surrounded by their preferred fluid, regardless of their relative surface areas. To achieve this equilibrium orientation, the cylinders must be displaced vertically, causing the interface to no longer pass through the central-axis. Rotation about a line other than the central-axis would reduce the torques, as the moment arm is no longer defined by the diameter of the cylinder $2R$ but rather the cord length $2R\sin(\pi f)$. Yet, even with this consideration, we believe that tethering Janus particles can inhibit their rotational alignment with twists consistent with the capillary torques available.

Model of compliant Janus cylinders

To further explore the coupling between capillarity and torsion, we consider a variant geometry in which two Janus cylinders are directly connected to form a single antisymmetric element, which itself is compliant (Fig. 5a). When placed at a liquid interface, the capillary torques are no longer exerted at the two ends but rather distributed along the length creating a continuous variation of twist in the axial direction, which we refer to as a twist profile. For this continuous case, we find it clearer to denote the twist angle in radians rather than degrees. Because of the antisymmetric Janus configuration, the twist profile must also be antisymmetric about the element's midpoint, which is therefore a natural location to set the origin (Fig. 5a).

Focusing on the twist in the positive x-direction (Fig. 5a), we define the angle of twist such that $\phi = \pi/2$ occurs when the surface energy E_s is at a minimum (Fig.1a). The wettability causes a capillary torque $T = dE_s/d\phi$, which vanishes when $\phi = \pi/2$. However, in the event that the angle of twist were to exceed $\pi/2$, the capillary torque will reverse direction, seeking again the most energetically favorable state. Thus it is evident that the sign of the capillary torque depends on the angle of twist, alternating between a positive and negative value about the point $\phi = \pi/2$. Recalling the surface energy dE_s for Janus cylinders discussed earlier, it follows that the magnitude of the torque per unit length can be expressed as $t(\phi) = \gamma R(\cos\theta_1 - \cos\theta_2)$. For simplicity, we assume perfectly wetting and non-wetting surfaces, which reduce the torque per unit length to $t(\phi) = \pm 2\gamma R$, with $t(\phi = \pi/2) = 0$.

For the positive half of the cylinder $x > 0$, the equilibrium twist profile $\phi(x)$ subjected to the distributed capillary torque must satisfy the following governing equation:

$$GJ\frac{d^2\phi}{dx^2} + t(\phi) = 0\ ; \quad t(\phi) = \begin{cases} 2\gamma R & \text{if } \phi < \pi/2 \\ 0 & \text{if } \phi = \pi/2 \\ -2\gamma R & \text{if } \phi > \pi/2 \end{cases} \tag{2}$$

Simultaneously, the cylinder must satisfy the boundary conditions $\phi(0) = 0$ from antisymmetry and $\phi'(L) = 0$ from the absence of an applied external torque, where the prime denotes the derivative with respect to x. Solving Equation (2) with these boundary

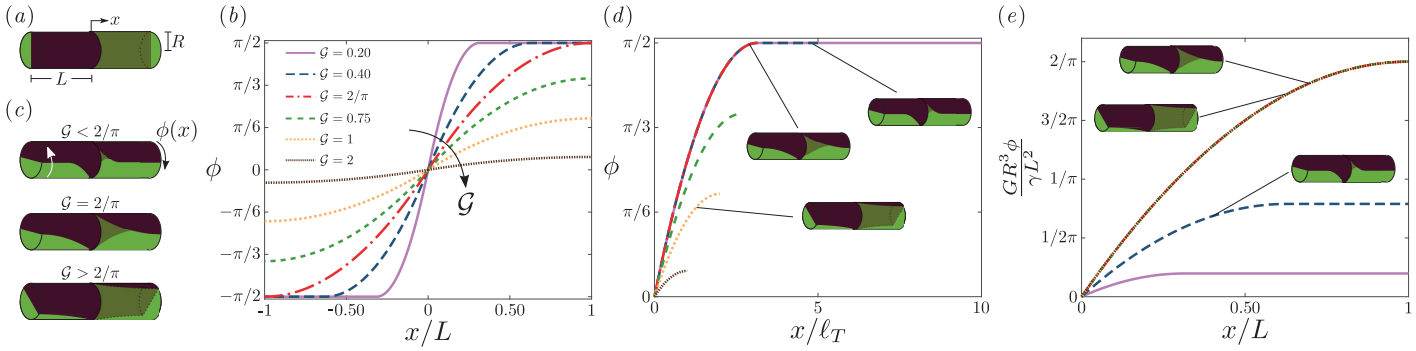

Fig. 5 Twist profiles of an antisymmetric element consisting of two connected, compliant Janus cylinders. ***a*** Schematic of the initial configuration of the antisymmetric element, with the origin located at its midpoint. ***b*** Twist angle as a function of the relative distance from the origin for increasing values of the dimensionless group $\mathcal{G} = \sqrt{GR^3/\gamma L^2}$. ***c*** Schematics of the twist profiles for three elements with increasing values of $\mathcal{G}$. ***d*** Twist angle against the position scaled by the torsional-capillary length ℓ_T. ***e*** Twist angle multiplied by $\mathcal{G}^2$ as a function of the relative position from the center x/L. Note that ϕ is displayed in radians for clarity.

conditions, we obtain an analytic expression for the twist profile:

$$\phi(x>0) = \begin{cases} \pi/2 & \text{if } \mathcal{G} \le \frac{2}{\pi} \text{ and } \frac{x}{L} \ge \frac{\pi}{2}\mathcal{G} \\ \frac{2x}{\pi \mathcal{G} L}(\pi - \frac{x}{\mathcal{G}L}) & \text{if } \mathcal{G} \le \frac{2}{\pi} \text{ and } \frac{x}{L} < \frac{\pi}{2}\mathcal{G} \\ \frac{2x}{\pi \mathcal{G}^2 L}(2 - \frac{x}{L}) & \text{if } \mathcal{G} > \frac{2}{\pi} \end{cases} \quad (3)$$

where $\mathcal{G} \equiv \sqrt{GR^3/\gamma L^2}$ is a dimensionless parameter that relates capillary and torsional effects. Note that the full solution also includes an equal and opposite twist profile for $x < 0$, following the antisymmetric condition $\phi(x) = -\phi(-x)$.

Because the governing equation for the twist profile is a quasi-linear boundary value problem, it is not surprising that we obtain a non-linear solution. The twist depends on the relative distance from the center x/L, as well as the value of $\mathcal{G}$, indicating the balance between torsion and capillarity (Fig. 5b). Elements with small values of $\mathcal{G}$ obtain a sharp twist profile, reaching $\phi = \pi/2$ and $-\pi/2$ for all points beyond a twisted region confined around the origin. These elements are sufficiently compliant that capillary forces overcome their torsional resistances. For increasing values of $\mathcal{G}$, the twist spreads out over a larger portion of the element until even the ends no longer fully rotate. At these larger values of $\mathcal{G}$, the element is sufficiently stiff that torsional resistance overwhelms the capillary forces. It should be noted that although the twist profile is continuous and smooth, the curvature is discontinuous such that the slope $\phi'(x)$ has kinks at the points when ϕ reaches $\pi/2$ and $-\pi/2$, as well as at the origin.

Mapping the non-linear solution onto the antisymmetric element can help visualize how the twisting profile dictates the equilibrium configuration (Fig. 5c). Here the color differentiates the hydrophobic and hydrophilic surfaces, resulting in an abrupt change in color at the origin that is unrelated to the twist. The sharp twist profile obtained for an element with a small value of $\mathcal{G}$ illustrates how most of the element fully reorients at equilibrium. The final orientation of the element is reminiscent of a regular Janus cylinder, apart from a small twisted region. The twist in that region increases quadratically with x until the maximum twist of $\pi/2$ is obtained at the point where the kinks occur in the slope. Increasing the value of $\mathcal{G}$ lengthens the twisted region until a critical value of $\mathcal{G} = 2/\pi$ is reached, indicating that there exists a characteristic length describing this twisted region. This characteristic length, the torsional-capillary length $\ell_T \equiv \sqrt{GR^3/\gamma}$ identifies the position where the surface and torsional forces balance. Indeed $\mathcal{G}$ can be interpreted as the torsional capillary length relative to the element length $\mathcal{G} = \ell_T/L$. For elements with values of $\mathcal{G}$ that exceeds the critical value, the balance between the surface and torsional forces occurs at a position beyond the length of the element L, and as a result the twist is confined by the ends. Note that the torsional-capillary length is analogous to the elasto-capillary length $\ell_E = \sqrt{Eh^3/\gamma}$ found in studies in which elastic structures are bent via capillary forces [1,6,25].

The twist profiles of the antisymmetric elements can be separated into two regimes based on which length scale, ℓ_T or L, is dominant. Rescaling the data from Figure 5b with the appropriate dimensionless groups can give us an insight for the two regimes. Plotting the twist ϕ against the position scaled with the torsional-capillary length x/ℓ_T reveals that the elements with the small values of $\mathcal{G}$ collapse into a single curve, whereas the curves with large values do not (Fig. 5d). If instead, the twist ϕ multiplied by $\mathcal{G}^2$ is plotted against the position relative to the length x/L, the elements with larger values of $\mathcal{G}$ collapse as a single curve, whereas curves with the small values do not (Fig. 5e). Thus by separating the solution into two regimes, the number of dimensionless parameters needed to characterize the twist profile can be reduced.

Conclusion

In summary, we have demonstrated how twist can be used to control the orientation of Janus particles at an air-water interface when tethered in an antisymmetric fashion. If compliant Janus cylinders are directly connected to form an antisymmetric element, then the twist can be solved by considering a distributed torque. For both geometries, the equilibrium configuration is dictated by the balance of the elastic and interfacial properties of the system and gives rise to a natural length scale, the torsional-capillary length. The competition between elastic and interfacial properties has been studied in many occasions involving bending of structures, and even in some cases bending coupled with twisting [26]. Here we have shown how pure twisting can be achieved through breaking rotational symmetry with variation in contact angle. Al-

though we have focused on solid cylinders, the approach described can also be applied to other configurations including bundles of fibers in functionalized fabrics. Additionally, tethers or antisymmetric elements could be designed to twist only under certain liquid conditions, including those that might swell the elastomer, and thus serve as sensing devices.

Acknowledgements

We thank H. A. Stone and L. Courbin for important early discussions, as well as P. Barbone for providing insight into how to formulate the free-boundary value problem. The research was partially supported by the National Science Foundation under Grant No. 1351466 and the Boston University Undergraduate Research Opportunities Program.

References

1 C. Py, P. Reverdy, L. Doppler, J. Bico, B. Roman and C. N. Baroud, *Phys. Rev. Lett.*, 2007, **98**, 156103.

2 A. Antkowiak, B. Audoly, C. Josserand, S. Neukirch and M. Rivetti, *Proc. Natl. Acad. Sci.*, 2011, **108**, 10400–10404.

3 J. Huang, M. Juszkiewicz, W. H. De Jeu, E. Cerda, T. Emrick, N. Menon and T. P. Russell, *Science*, 2007, **317**, 650–653.

4 M. Pineirua, N. Tanaka, B. Roman and J. Bico, *Soft Matter*, 2013, **9**, 10985–10992.

5 A. Fargette, S. Neukirch and A. Antkowiak, *Phys. Rev. Lett.*, 2014, **112**, 137802.

6 B. Roman and J. Bico, *J. Phys. Condens. Matter*, 2010, **22**, 493101.

7 B. Binks and S. Lumsdon, *Langmuir*, 2000, **16**, 8622–8631.

8 S. U. Pickering, *Journal of the Chemical Society, Transactions*, 1907, **91**, 2001–2021.

9 C. Casagrande, P. Fabre, E. Raphael and M. Veyssie, *Europhys. Lett.*, 1989, **9**, 251.

10 T. Ondarçuhu, P. Fabre, E. Raphaël and M. Veyssié, *J. Phys. France*, 1990, **51**, 1527–1536.

11 B. Binks and P. Fletcher, *Langmuir*, 2001, **17**, 4708–4710.

12 N. Glaser, D. J. Adams, A. Böker and G. Krausch, *Langmuir*, 2006, **22**, 5227–5229.

13 T. Nisisako, T. Torii, T. Takahashi and Y. Takizawa, *Advanced Materials*, 2006, **18**, 1152–1156.

14 J. R. Howse, R. A. Jones, A. J. Ryan, T. Gough, R. Vafabakhsh and R. Golestanian, *Phys. Rev. Lett.*, 2007, **99**, 048102.

15 A. Kumar, B. J. Park, F. Tu and D. Lee, *Soft Matter*, 2013, **9**, 6604–6617.

16 D. J. Adams, S. Adams, J. Melrose and A. C. Weaver, *Colloids Surf. A: Physicochem. Eng. Aspects (2016)*, 2008, **317**, 360–365.

17 H. Rezvantalab, K. W. Connington and S. Shojaei-Zadeh, *Phys. Rev. Fluids*, 2016, **1**, 074205.

18 H. Rezvantalab and S. Shojaei-Zadeh, *ACS Nano*, 2016, **10**, 5354–5361.

19 R. S. Rivlin, *J. Appl. Phys.*, 1947, **18**, 444–449.

20 P.-G. De Gennes, F. Brochard-Wyart and D. Quéré, *Capillarity and wetting phenomena: drops, bubbles, pearls, waves*, Springer Science & Business Media, 2013.

21 A. C. Ugural and S. K. Fenster, *Advanced strength and applied elasticity*, Pearson Education, 2003.

22 R. H. Pritchard, P. Lava, D. Debruyne and E. M. Terentjev, *Soft Matter*, 2013, **9**, 6037–6045.

23 A. E. H. Love, *A treatise on the mathematical theory of elasticity*, Cambridge university press, 1927.

24 B. Audoly, *Introduction to the Elasticity of Rods. In C. Duprat and H. A. Stone, editors,*, Royal Society of Chemistry, 2015.

25 J. Bico, B. Roman, L. Moulin and A. Boudaoud, *Nature*, 2004, **432**, 690–690.

26 A. Legrain, E. J. Berenschot, L. Abelmann, J. Bico and N. R. Tas, *Soft Matter*, 2016, **12**, 7186–7194.